European Conference on Optical Communication (ECOC) 2022 © Optica Publishing Group 2022

High-Bandwidth Lithium Niobate Electro-Optic Modulator at Visible-Near-Infrared Wavelengths

David Pohl(1), Jost Kellner(1), Fabian Kaufmann(1), Alfonso Martínez-García(1,2), Giovanni Finco(1), Andreas Maeder(1), Marc Reig-Escalé(1,2) and Rachel Grange(1)

(1) ETH Zürich, Department of Physics, Institute for Quantum Electronics, Optical Nanomaterial Group, 8093 Zurich, Switzerland dpohl@phys.ethz.ch
(2) Versics AG, 8093 Zurich, Switzerland marc.reig@versics.com

Abstract *Lithium niobate on insulator is presented as a platform for active integrated photonics at visible-near-infrared wavelengths. An electro-optic modulator operating at 780 nm featuring an electrical 3-dB bandwidth of 35 GHz and a halfwave voltage of 2.82 V is demonstrated, enabling transmission of a 40 Gbit/s on-off keying signal. ©2022 The Author(s)*

Introduction

Integrated photonic circuits and devices working at visible-near-infrared wavelengths promise to be a viable approach for scaling up optical systems used in free-space optical (FSO) communication, sensing and quantum optics. For example, integrated electro-optic modulators operating at wavelengths around 750-850 nm could enhance the performance of FSO satellite downlinks or inter-satellite links[1]–[3] as well as radio-over-FSO (RoFSO) systems based on a hybrid fiber-FSO link[4],[5]. Nowadays, visible-near-infrared modulators are also crucial components for quantum computing based on trapped ions or atoms with transition energies in this wavelength range[6],[7]. However, scaling up the schemes to address multiple ions or atoms is limited by the complexity of the conventionally used free-space optical systems involving discrete components. Integrated devices and circuits could overcome this bottleneck by enabling small-footprint, stable and scalable alternatives[8]. Additionally, integrated photonics in the visible has been employed for applications in spectroscopy[9], optical biosensing[10] or precision metrology on a chip[11].

Since silicon is absorbing below wavelengths of 1100 nm, the well-established silicon photonics platform based on CMOS fabrication processes is not applicable for visible-near-infrared wavelengths. Various materials have been studied to realize integrated photonics in this wavelength range, including SiN[12], SiO_2[13], AlN[14], diamond[15], lithium niobate[16] and hybrid approaches (SiN/LN)[17]. Of these materials, only lithium niobate (LN) and AlN allow for electro-optically active devices. However, due to the relatively low electro-optic coefficient of AlN ($\sim$1 pm/V[14]) compared to LN ($\sim$30 pm/V), LN is an attractive material to realize high bandwidth electro-optic modulators at low driving voltages in the visible-near-infrared regime. Lithium niobate on insulator (LNOI) has emerged in past years as a versatile platform for low-loss integrated photonics with applications in optical communications[18],[19], nonlinear optics[20] and quantum optics[21]. Nevertheless, the vast majority of studies on LNOI focus on wavelengths around 1550 nm and only few works on integrated photonics in LNOI at visible-near-infrared wavelengths have been reported[16],[22],[23].

Here, we present the optical design and fabrication of integrated photonic circuits in LNOI at wavelengths around 780 nm and demonstrate a 4.5 mm long electro-optical Mach-Zehnder modulator (MZM) with an electrical bandwidth of 35 GHz and a halfwave voltage of 2.82 V, corresponding to a halfwave-length product of 1.27 V·cm. We study the design of the coplanar waveguide (CPW) for the MZM with respect to impedance and velocity matching at this operating wavelength range and characterize the fabricated MZMs electrically and electro-optically. Finally, we perform data transmission experiments with non-return to zero on-off keying (NRZ-OOK) signals and record open eye diagrams up to 40 Gbit/s.

Optical Design and Device Fabrication

In this section, the design considerations for realizing integrated photonic circuits in the visible using LNOI are introduced. Fig. 1(a) shows a schematic of a waveguide MZM including two 1×2 multimode interferometers (MMIs) and a coplanar waveguide (CPW) as the RF transmission line. The first design choice to be made

European Conference on Optical Communication (ECOC) 2022 © Optica Publishing Group 2022

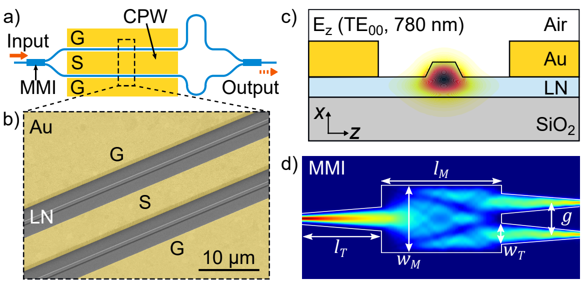

Fig. 1: (a) Schematic of a Mach-Zehnder modulator (MZM) including two multimode interferometers (MMIs) and a coplanar waveguide (CPW) to couple the microwave and optical signals. b) SEM image of the electro-optic interaction region showing two lithium niobate on insulator (LNOI) waveguides in the gaps of a gold CPW. (c) Cross-section of an LNOI waveguide with the simulated electric field component along the crystal z-axis of the TE_{00} mode at 780 nm. (d) Simulated mode distribution for an 1×2-MMI.

are the waveguide dimensions. Here, we use a 300 nm x-cut LN thin-film on top of a 4.7 µm thick SiO_2 layer on a silicon substrate. For an etch depth of 150 nm we choose a waveguide top width of 400 nm in order to obtain single-mode waveguides for TE polarization with an optical group index of n_o = 2.4. The simulated electric field along the extraordinary crystal z-axis of the fundamental TE mode is shown in Fig. 1(c) together with the cross-section of a LNOI waveguide placed inbetween a pair of gold electrodes. The second optical building block is the 1×2 MMI, which is designed using a bidirectional eigenmode solver to minimize the excess loss for the wavelength range of interest. The simulated mode profile is shown in Fig. 1(d) and the relevant design parameters are indicated. We reported measured excess loss of ∼0.2 dB per MMI for an etch depth of 115 nm elsewhere[24]. For an etch depth of 150 nm we adjusted the MMI parameters to the following: l_M = 72.4 µm, w_M = 7 µm, l_T = 90 µm, w_T = 2.2 µm and g = 3.5 µm. An SEM image of a device fabricated with the same process flow as reported previously[19] is shown in Fig. 1(b).

Electrical Device Design and Characterization

Bandwidth limitations of travelling-wave MZMs are mainly due to RF losses, velocity and impedance mismatch[25]. Hence, the design of the CPW is crucial to balance the bandwidth-voltage tradeoff. In Fig. 2(a) the cross-section of a CPW on LNOI is shown and the realized devices had an electrode thickness t of 0.9 µm, a gap of 5.2 µm and a ground width w_g above 200 µm. In Figs. 2(b)-(d) we show the electrical characterization of two CPWs with signal widths w_s of 5 µm and 30 µm, measured using a 67 GHz vector network analyser (VNA) and a pair of GSG microwave probes. Lower RF losses, impedance matching to 50 Ω and a higher RF phase index is expected from simulations for the 30 µm signal line, which is verified by the measurements. However, the RF phase index of ∼2 is still substantially lower than the optical group index at 2.4. Hence, by using simple CPW structures, velocity and impedance matching for a MZM at 780 nm is not simultaneously achievable for the given LNOI material stack and waveguide dimensions.

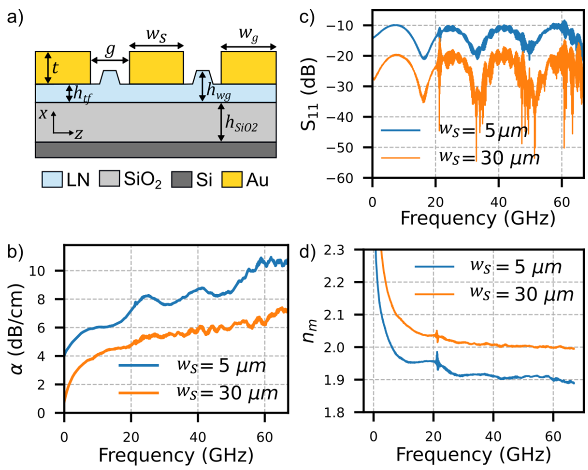

Fig. 2: (a) Cross-section of the electro-optic interaction region of a Mach-Zehnder modulator (MZM). The dimensional parameters of the material stack and the coplanar waveguide (CPW) used in this work are specified in the text. (b) Measured RF losses for two CPWs with different signal widths w_s. (c) Measured electrical reflections S_{11}. (d) Measured RF phase indices.

Electro-Opic Measurements

In order to measure the DC characteristics and the electro-optic response of the MZMs we used the setup sketched in Fig. 3(a). For the DC or low-frequency characterization we applied a 1 kHz triangular voltage signal to the MZMs while recording the transmitted optical intensity. Fig. 3(b) shows the obtained normalized transmission versus applied voltage for a 4.5 mm long CPW. The halfwave voltage is 2.82 V, corresponding to a voltage-length product of 1.27 V·cm, and the optical extinction ratios were typically around 20 dB. The electro-optic response shown in Fig. 3(c) was measured using the VNA and a 45 GHz photodiode. The cables and GSG microwave probes were de-embedded by performing a calibration using an impedance standard substrate. As expected from the electrical characterization of the CPWs in the previous section, the MZM with the 30 µm signal electrode showed a larger electrical 3-dB bandwidth (corresponding to the optical 1.5-dB bandwidth[25]) of ∼35 GHz and an opti-

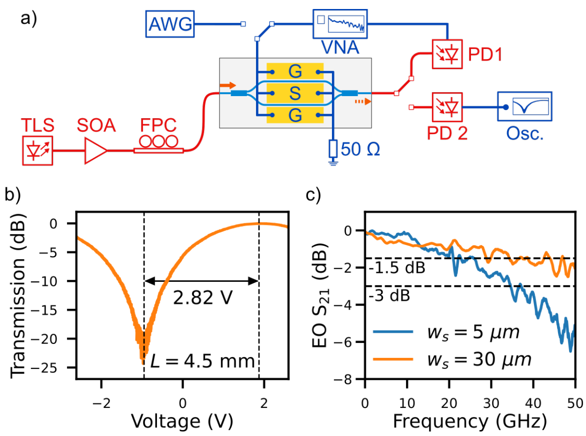

Fig. 3: (a) Setup for DC characterization and electro-optic (EO) response measurements including a tunable laser source (TLS), a semiconductor optical amplifier (SOA) and a fiber polarization controller (FPC). The coplanar waveguide (CPW) is contacted using a pair of GSG microwave probes, one of which is used to terminate the transmission line. An arbitrary waveform generator (AWG) and a slow photodiode (PD2) are used for the DC characterization. The obtained normalized transmission is shown in (b) with a halfwave voltage of 2.82 V for a 4.5 mm long MZM. The small-signal EO responses of two MZMs with different signal widths w_s are plotted in (c). These results were measured using a 67 GHz vector network analyser (VNA) and a 45 GHz photodiode (PD1).

cal 3-dB bandwidth beyond 50 GHz. Also, the steeper roll-off at high frequencies of the MZM with the 5 µm signal line due to the larger velocity mismatch is observed. At frequencies below 12 GHz, the narrow MZM shows peaking in the electro-optic response caused by an impedance larger than 50 Ω.

Data Transmission Experiments

Finally, we performed NRZ-OOK data modulation experiments using the setup sketched in Fig. 4(a). A pseudo-random binary sequence (PRBS) is generated by a digital-to-analog converter (DAC) with a sampling rate of 100 GS/s, a peak-to-peak output voltage up to 500 mV_{pp} and a 3-dB bandwidth of 44 GHz. The electrical signal is then amplified and applied to the device using a GSG microwave probe. The peak-to-peak voltage after the microwave probe was around 2 V_{pp}, depending on the output voltage of the DAC and the data rate. Light from a tunable laser source (TLS) at 780 nm is amplified to ∼25 dBm using a semiconductor optical amplifier before being coupled to the integrated MZM using a lensed fiber. The modulated optical signal at the output is collected and measured using a 25 GHz photoreceiver with a transimpedance amplifier and a real-time oscilloscope (RTO) with a sampling rate of 100 GS/s and an analog bandwidth of 33 GHz. We used such high optical input powers due to large optical coupling losses. Nevertheless, we achieved

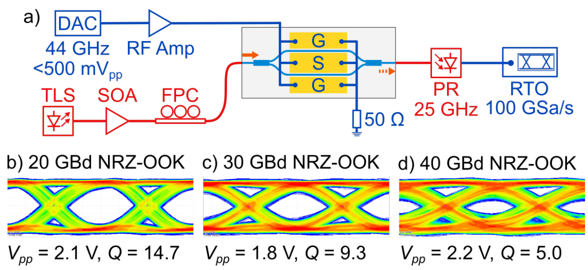

Fig. 4: (a) Setup for the data transmission measurements. A digital-to-analog converter (DAC) generates the NRZ-OOK pseudo-random binary sequence which is amplified using an RF amplifier. The intensity modulated optical signal is detected with a 25 GHz photoreceiver (PR) and a real-time oscilloscope (RTO). In (b)-(d), exemplary eye diagrams for NRZ-OOK modulation at 20 Gbit/s, 30 Gbit/s and 40 Gbit/s are shown, respectively. The corresponding peak-peak voltages V_{pp} fed to the device and the resulting Q-factors are displayed.

open eye diagrams for NRZ-OOK signals up to data rates of 40 Gbit/s without forward error correction, limited by the RTO and the photoreceiver. In Figs. 4(b)-(d) the recorded eye diagrams for 20 Gbit/s, 30 Gbit/s and 40 Gbit/s are shown for the MZM with the 5 µm wide signal electrode, which showed lower insertion losses. The measured Q-factors were 14.7, 9.3 and 5.0, corresponding to bit error ratios (BERs) on the order of 10^{-49}, 10^{-20} and 10^{-7}, respectively, and the on-chip applied peak-to-peak voltages are indicated.

Conclusion

We have demonstrated the potential of LNOI as a platform for scalable passive and active integrated photonic circuits at visible-near-infrared wavelengths. Fabricated electro-optic MZMs with 4.5 mm long CPWs showed an electrical 3-dB bandwidth of 35 GHz and a halfwave voltage of 2.82 V at an operating wavelength of 780 nm. Also, NRZ-OOK data modulation experiments with open eye diagrams up to 40 Gbit/s are reported. In order to enhance the bandwidth of visible MZMs while maintaining low driving voltages, more sophisticated CPW designs could be employed to allow for simultaneous velocity and impedance matching and changing the substrate material to quartz or sapphire would drastically reduce the RF losses[23],[26]. Due to the integrated nature of the demonstrated devices, more complex photonic circuits such as cascaded MZMs to increase the extinction ratio are feasible.

Acknowledgements

We acknowledge the support for nanofabrication from ScopeM, BRNC and FIRST of ETH Zürich and funding from ESA Co-funded Research and SNSF BRIDGE Discovery 194693.

References

[1] A. Carrasco-Casado and R. Mata-Calvo, "Space Optical Links for Communication Networks", in *Springer Handbook of Optical Networks*, Cham, Switzerland: Springer International Publishing, 2020, pp. 1057–1103. DOI: 10.1007/978-3-030-16250-4_34.

[2] M. I. Shehata, M. Asmaa Zaki, H. A. Fayed, A. A. E. Aziz, and M. H. Aly, "Optical Inter-Satellite Link over Low Earth Orbit: Enhanced Performance", *Journal of Physics: Conference Series*, vol. 2128, no. 1, p. 012 001, Dec. 2021. DOI: 10.1088/1742-6596/2128/1/012001.

[3] D. Giggenbach, J. Horwath, and B. Epple, "Optical Satellite Downlinks to Optical Ground Stations and High-Altitude Platforms", in *2007 16th IST Mobile and Wireless Communications Summit*, Jul. 2007, pp. 1–4. DOI: 10.1109/ISTMWC.2007.4299318.

[4] A. B. Raj and A. K. Majumder, "Historical perspective of free space optical communications: From the early dates to today's developments", *IET Communications*, vol. 13, no. 16, pp. 2405–2419, 2019. DOI: 10.1049/iet-com.2019.0051.

[5] A. Jurado-Navas, A. Tatarczak, X. Lu, J. J. V. Olmos, J. M. Garrido-Balsells, and I. T. Monroy, "850-nm hybrid fiber/free-space optical communications using orbital angular momentum modes", *Optics Express*, vol. 23, no. 26, pp. 33 721–33 732, Dec. 2015. DOI: 10.1364/OE.23.033721.

[6] K. Wright, K. M. Beck, S. Debnath, *et al.*, "Benchmarking an 11-qubit quantum computer", *Nature Communications*, vol. 10, no. 1, p. 5464, Dec. 2019. DOI: 10.1038/s41467-019-13534-2.

[7] R. Dumke, M. Volk, T. Müther, F. B. J. Buchkremer, G. Birkl, and W. Ertmer, "Micro-optical Realization of Arrays of Selectively Addressable Dipole Traps: A Scalable Configuration for Quantum Computation with Atomic Qubits", *Physical Review Letters*, vol. 89, no. 9, p. 097 903, Aug. 2002. DOI: 10.1103/PhysRevLett.89.097903.

[8] K. K. Mehta, C. Zhang, M. Malinowski, T.-L. Nguyen, M. Stadler, and J. P. Home, "Integrated optical multi-ion quantum logic", *Nature*, vol. 586, no. 7830, pp. 533–537, Oct. 2020. DOI: 10.1038/s41586-020-2823-6.

[9] A. Dhakal, P. C. Wuytens, F. Peyskens, K. Jans, N. L. Thomas, and R. Baets, "Nanophotonic Waveguide Enhanced Raman Spectroscopy of Biological Submonolayers", *ACS Photonics*, vol. 3, no. 11, pp. 2141–2149, Nov. 2016. DOI: 10.1021/acsphotonics.6b00593.

[10] P. Muellner, E. Melnik, G. Koppitsch, J. Kraft, F. Schrank, and R. Hainberger, "CMOS-compatible Si3N4 Waveguides for Optical Biosensing", *Procedia Engineering*, Eurosensors 2015, vol. 120, pp. 578–581, Jan. 2015. DOI: 10.1016/j.proeng.2015.08.728.

[11] J. Kitching, E. A. Donley, S. Knappe, *et al.*, "NIST on a Chip: Realizing SI units with microfabricated alkali vapour cells", *Journal of Physics: Conference Series*, vol. 723, p. 012 056, Jun. 2016. DOI: 10.1088/1742-6596/723/1/012056.

[12] S. Romero-García, F. Merget, F. Zhong, H. Finkelstein, and J. Witzens, "Silicon nitride CMOS-compatible platform for integrated photonics applications at visible wavelengths", *Optics Express*, vol. 21, no. 12, pp. 14 036–14 046, Jun. 2013. DOI: 10.1364/OE.21.014036.

[13] Y. Gong and J. Vučković, "Photonic crystal cavities in silicon dioxide", *Applied Physics Letters*, vol. 96, no. 3, p. 031 107, Jan. 2010. DOI: 10.1063/1.3297877.

[14] S. Zhu, Q. Zhong, T. Hu, *et al.*, "Aluminum Nitride Ultralow Loss Waveguides and Push-Pull Electro-Optic Modulators for Near Infrared and Visible Integrated Photonics", in *2019 Optical Fiber Communications Conference and Exhibition (OFC)*, Mar. 2019, pp. 1–3.

[15] B. J. M. Hausmann, B. Shields, Q. Quan, *et al.*, "Integrated Diamond Networks for Quantum Nanophotonics", *Nano Letters*, vol. 12, no. 3, pp. 1578–1582, Mar. 2012. DOI: 10.1021/nl204449n.

[16] B. Desiatov, A. Shams-Ansari, M. Zhang, C. Wang, and M. Lončar, "Ultra-low-loss integrated visible photonics using thin-film lithium niobate", *Optica*, vol. 6, no. 3, pp. 380–384, Mar. 2019. DOI: 10.1364/OPTICA.6.000380.

[17] K. K. Mehta, G. N. West, and R. J. Ram, "SiN-on-LiNbO3 integrated optical modulation at visible wavelengths", in *2017 Conference on Lasers and Electro-Optics (CLEO)*, May 2017.

[18] M. Zhang, C. Wang, P. Kharel, D. Zhu, and M. Lončar, "Integrated lithium niobate electro-optic modulators: When performance meets scalability", *Optica*, vol. 8, no. 5, pp. 652–667, May 2021. DOI: 10.1364/OPTICA.415762.

[19] D. Pohl, A. Messner, F. Kaufmann, *et al.*, "100-GBd Waveguide Bragg Grating Modulator in Thin-Film Lithium Niobate", *IEEE Photonics Technology Letters*, vol. 33, no. 2, pp. 85–88, Jan. 2021. DOI: 10.1109/LPT.2020.3044648.

[20] M. Reig Escalé, F. Kaufmann, H. Jiang, D. Pohl, and R. Grange, "Generation of 280 THz-spanning near-ultraviolet light in lithium niobate-on-insulator waveguides with sub-100 pJ pulses", *APL Photonics*, vol. 5, no. 12, p. 121 301, Dec. 2020. DOI: 10.1063/5.0028776.

[21] S. Saravi, T. Pertsch, and F. Setzpfandt, "Lithium Niobate on Insulator: An Emerging Platform for Integrated Quantum Photonics", *Advanced Optical Materials*, vol. 9, no. 22, p. 2 100 789, 2021, ISSN: 2195-1071. DOI: 10.1002/adom.202100789.

[22] C. Li, B. Chen, Z. Ruan, P. Chen, K. Chen, and C. Guo, *High Modulation Efficiency and Large Bandwidth Thin-Film Lithium Niobate Modulator for Visible Light*, 2022. arXiv: 2202.13323.

[23] O. T. Celik, C. J. Sarabalis, F. M. Mayor, *et al.*, *High-bandwidth CMOS-voltage-level electro-optic modulation of 780 nm light in thin-film lithium niobate*, Apr. 2022. arXiv: 2204.03138.

[24] D. Pohl, J. Kellner, F. Kaufmann, A. Maeder, M. Reig-Escale, and R. Grange, "Multimode Interferometer in Lithium Niobate-on-Insulator centered at 780 nm", in *Accepted for 22 Conference on Lasers and Electro-Optics (CLEO)*, San Jose, California, May 2022.

[25] G. Ghione, *Semiconductor Devices for High-Speed Optoelectronics*. Cambridge: Cambridge University Press, 2009. DOI: 10.1017/CBO9780511635595.

[26] P. Kharel, C. Reimer, K. Luke, L. He, and M. Zhang, "Breaking voltage–bandwidth limits in integrated lithium niobate modulators using micro-structured electrodes", *Optica*, vol. 8, no. 3, p. 357, Mar. 2021. DOI: 10.1364/OPTICA.416155.